EXPERIMENTAL STABILITY STUDY ON HERRINGBONE-MICROGROOVED JOURNAL BEARING IN AN IMPELLER-SPINDLE

B.-H. Chang * **P.-H. Chen**

Department of Mechanical Engineering
National Taiwan University
Taipei, Taiwan 10617, R.O.C.

D.-S. Lee

Department of Energy and Refrigerating Air Conditioning Engineering
National Taipei University of Technology
Taipei, Taiwan 10617, R.O.C.

ABSTRACT

The reliability of the impeller-spindle with respect to the effects of abnormal vibrations and noises is relative to the whirl rotation in notebook (NB) computers, all-in-one (AIO) desktop systems, and tablet PCs. This study experimentally investigates the stability of a herringbone-microgrooved journal bearing in an impeller-spindle under static radial forces. The experimental device operated at 2700, 3600, 4200, and 4900rpm, with a static load ranging from 0.4, 0.8, and 1.6N. The experiment obtained the stiffness and damping coefficients, and the study involved analyzing the stability. Results show that the dimensionless threshold speed of rotation decreased as the Sommerfeld number increased. The proposed impeller-spindle is stable when the Sommerfeld number is less than 59, indicating that the impeller-spindle should not operate at an eccentricity ratio below 0.18.

Keywords: Herringbone-microgrooved journal bearing, Impeller-spindle, Stability, Dimensionless threshold speed of rotation.

1. INTRODUCTION

Numerous researchers have investigated the stiffness and damping coefficients of various designs of hydrodynamic bearings, such as plain journal bearing, pivot tilt pad journal bearing, and herringbone-microgrooved journal bearing, to improve the characteristics of rotor dynamics. Matsud *et al*. [1] proposed a criterion for optimizing the configuration of a fluid-film plain journal bearing for stability improvement. This standard aims to minimize the magnitude of the cross-coupling terms of stiffness coefficients. As for stability characteristics, whirl instability does not occur for the designed bearings over all eccentricity ratios. Ono *et al*. [2] analyzed the stability of a disk-spindle supported by a plain journal bearing, and pivot bearing increases quadratically as rotational speed increases. Zhou *et al*. [3] studied the oil-film dynamic coefficients of a journal bearing using an experimental method. They evaluated the dynamic coefficients employing the least mean squares method under different static and dynamic loads. Ertas *et al*. [4] described the effects of same sign-stiffness cross-coupling rotordynamic stability, showing that the presence of cross –coupled stiffness (CCS) does not always imply a destabilizing influence on rotordynamic whirls. The traditional approach of stability analysis related to spindle motors with a herringbone herringbone-microgrooved journal bearing focuses on hard disk drive (HDD) applications. Numerous researchers have studied the dynamic characteristics and stability analysis of HDD systems using simulation methods. For example, Jang *et al*. [5,6] investigated the nonlinear dynamic analysis of a hydrodynamic journal bearing. They determined dynamic behaviors, such as orbit or rotational speed, by solving nonlinear equations of motion. Another analytical method shows that the instability of hydrodynamic journal bearing with rotating herringbone herringbone-grooves increases alongside eccentricity, while decreasing groove number. Hwang *et al*. [7] implemented numerical methods to analyze three types of hydrodynamic journal air bearings for high performance HDD spindles, comparing their performances according to pressure distribution, load capacity, radial stiffness, unbalance response, and stability threshold. Rao *et al*. [8] proposed a method for calculating the

* Corresponding author (paul_chang@avc.com.tw)

DOI : 10.1017/jmech.2012.13
Copyright © 2012 The Society of Theoretical and Applied Mechanics, R.O.C.
https://doi.org/10.1017/jmech.2012.13 Published online by Cambridge University Press

stability characteristics of herringbone-microgrooved journal bearing incorporating cavitation effects, but focused only on stability with geometry parameters of herringbone herringbone-microgrooved journal bearing. Chu *et al*. [9] presented a modified molecular gas lubrication equation including the effect of gas rarefaction, solved using the finite-element method to obtain dynamic pressure distribution and dynamic coefficients. Few researchers have experimentally investigated the dynamic characteristics of HDD systems with the herringbone-microgrooved journal bearing. Jintanawan [10] presented a dynamic model of a disk-spindle system with distributed forces in herringbone-microgrooved journal bearing for predicting the transverse vibrations of HDD spindles. Miwa *et al*. [11] proposed a new method for evaluating the damping and frequency characteristics of fluid dynamic bearing (FDB) spindle, using a high-frequency vibration base. Jang *et al*. [12] studied the development of HDD spindle motor with increased stiffness and damping coefficients, using a stationary permanent magnet in sleeve. Stationary magnetic forces increase the stiffness and damping effects of hydrodynamic bearings. Nemat-Alla *et al*. [13] experimentally investigated the static and dynamic characteristics of beveled-step herringbone-microgrooved journal bearing and bearing attitude angle, pressure distribution, and bearing friction torque were measured. Their results show that higher eccentricity ratios achieve better stability for beveled-step herringbone-microgrooved journal bearings compared to plain journal bearing. Lui *et al*. [14] proposed multi-step herringbone-grooved journal bearing for data storage devices, to reduce abrasion between the spindle and bearing by CFD software and experimental verification.

In recent years, herringbone-microgrooved journal bearing has rapidly replaced ball bearings not only in HDD applications, but also in the impeller-spindle used for heat dissipation of microprocessors in notebook (NB) computers, all-in-one (AIO) desktop systems, and tablet PCs. Herringbone-microgrooved journal bearing is significant improvements in terms of reliability for impeller-spindle, regarding abnormal vibrations and acoustic noises. The static radial force of an impeller varies in magnitude and direction with the rated speed of the impeller-spindle and portable operation direction. The static radial force is a dominant factor of static load and causes the dynamic properties of an impeller-spindle to vary considerably, significantly affecting the stability characteristics. Improving herringbone-microgrooved journal bearing reliability, vibration and acoustics capability due to the effects of self-excited whirl in herringbone-microgrooved journal bearing requires determining if the impeller-spindle operates within the stability region.

This study experimentally investigates the stability of an impeller-spindle supported by a herringbone-microgrooved journal bearing under static loads, examining the dimensionless threshold speed of rotation and the ratio of dimensionless critical mass to dimensionless mass at various given Sommerfeld numbers [15], defined as $S = \mu NLD/W(R/C)^2$. The experimental procedures reveal the dynamic coefficients of stiffness and damping, and derive the stability characteristics of the system for stability analysis. The rest of the study is organized as follows: Section 2 shows the geometry parameters of the herringbone-microgrooved bearing and the impeller-spindle used in the experiment, Section 3 presents the methods to determine stiffness and damping coefficients of the system for stability analysis, Section 4 provides the experimental apparatus and operation procedures for data acquisition, Section 5 presents the results and discussions, and finally, Section 6 offers conclusions.

2. EXPERIMENTAL DESIGN FOR THE IMPELLER-SPINDLE WITH A HERRINGBONE-MICROGROOVED JOURNAL BEARING

Considering the physical configuration of the impeller-spindle shown in Fig. 1, the main components include an impeller as a rotating part, a stator, and a herringbone-microgrooved journal bearing. To overcome the difficulty of directly measuring the displacement of rotating shafts and determining the dynamic coefficients due to the impeller being contained within the fan housing, the experimental impeller-spindle shown in Fig. 2 was designed accordingly. Electromagnetic forces attract the metal ring enclosing the rotor, enabling the simulation of the static loads on the impeller when the impeller-spindle operates in NB, AIO PC, and tablet PC systems. The proposed impeller-spindle keeps mass unbalance under 0.04g-mm, and the rotor is loaded symmetrically to confirm that the tilt angle is under 0.002°, ensuring that the rotor inertia effect due to the transverse and polar mass moment is negligible. The herringbone-microgrooved patterns in Fig. 3 were cut on a conventional center lathe. The key geometry parameters include the groove angle β, the radial clearance of the journal bearing C, the groove depth C_g, the ridge width W_r, and the groove width W_g. Table 1 lists the related specifications of the herringbone-microgrooved journal bearing.

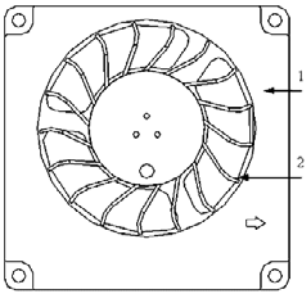
3. EXPERIMENTAL IDENTIFICATION METHOD FOR STABILITY CHARACTERISTICS

This section introduces the model for stability analysis and the considered parameters.

3.1 Stability Characteristics

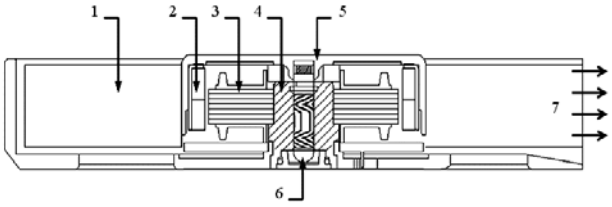
Based on the direct approach to stability analysis by San Andrés [16], Eq. (1) shows the dimensionless equations of motion for impeller-spindle supported on herringbone-microgrooved journal bearing:

https://doi.org/10.1017/jmech.2012.13 Published online by Cambridge University Press



1. Fan housing 2. Impeller

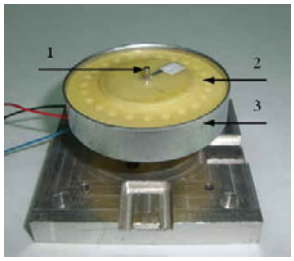
(a) Top view of the model



1. Impeller 2. Magnet 3. Stator 4. Herringbone-microgrooved journal bearing 5. Hub 6. Journal 7. Direction of outflow

(b) Cross section of the model

Fig. 1 Configuration of the impeller-spindle



1. Shaft 2. Rotor 3. Metal ring

Fig. 2 Experiment of impeller-spindle

$$\bar{M}\begin{bmatrix}\ddot{\bar{x}}\\ \ddot{\bar{y}}\end{bmatrix}+\begin{bmatrix}c_{XX} & c_{XY}\\ c_{YX} & c_{YY}\end{bmatrix}\begin{bmatrix}\dot{\bar{x}}\\ \dot{\bar{y}}\end{bmatrix}+\begin{bmatrix}k_{XX} & k_{XY}\\ k_{YX} & k_{YY}\end{bmatrix}\begin{bmatrix}\bar{x}\\ \bar{y}\end{bmatrix}=\bar{M}\eta\begin{bmatrix}\cos\tau\\ \sin\tau\end{bmatrix} \quad (1)$$

where the dimensionless variables are:

$$\bar{x}=\frac{\Delta x}{C};\ \bar{y}=\frac{\Delta y}{C};\ \tau=\Omega t;\ \eta=\frac{r_c}{C};\ \left(\bullet\right)=\frac{d}{d\tau} \quad (2)$$

and the dimensionless dynamic coefficients are:

$$k_{ij}=\frac{K_{ij}C}{W};\quad c_{ij}=\frac{C_{ij}C\Omega}{W} \quad (3)$$

The term C is the radial clearance of the journal bearing, W is the static load, and Ω is the rotational speed of the impeller-spindle. $\bar{M}=\frac{CM\Omega^2}{W}$ represents the dimensionless mass, where M is rotor mass. Considering that the system is stable due to the small amplitude journal motions around the equilibrium position, the dimensionless equations of motion for the impeller-spindle can be retrieved as:

Table 1 Design parameters of the herringbone-microgrooved journal bearing

radius of journal	R	0.996 mm
number of grooves	N_g	6
radial clearance of journal bearing	C	2μm
groove angle	β	22.5
groove depth	C_g	9μm
groove depth ratio	$C_g/(C+C_g)$	0.82
ridge width	W_r	700μm
groove width ratio	$W_r/(W_r+W_g)$	0.67
upper groove length	L_1	1mm
lower groove length	L_2	0.8 mm
free groove length	L_3	1.75mm
width of journal bearing	L	5.35mm
dynamic viscosity of the lubricant	μ	0.197kg/m-s

$$\bar{M}\begin{bmatrix}\ddot{\bar{x}}\\ \ddot{\bar{y}}\end{bmatrix}+\begin{bmatrix}c_{XX} & c_{XY}\\ c_{YX} & c_{YY}\end{bmatrix}\begin{bmatrix}\dot{\bar{x}}\\ \dot{\bar{y}}\end{bmatrix}+\begin{bmatrix}k_{XX} & k_{XY}\\ k_{YX} & k_{YY}\end{bmatrix}\begin{bmatrix}\bar{x}\\ \bar{y}\end{bmatrix}=\begin{bmatrix}0\\ 0\end{bmatrix} \quad (4)$$

The impeller-spindle becomes unstable at a threshold speed of rotation Ω_s causing the rotor to perform undamped orbital motions at threshold of whirl frequency ω_s. Therefore, the trajectory of orbit motion satisfies the following equations:

$$\bar{x}=Xe^{j\omega_s t}=Xe^{j\bar{\omega}_s\tau};\ \bar{y}=Ye^{j\omega_s t}=Ye^{j\bar{\omega}_s\tau};\ j=\sqrt{-1} \quad (5)$$

where $\bar{\omega}_s=\frac{\omega_s}{\Omega_s}$ is the threshold of whirl frequency ratio, meaning the ratio between the threshold of whirl frequency and the threshold speed of rotation. Consequently, substituting Eq. (5) into Eq. (4) leads to:

$$\begin{bmatrix}-\bar{M}_s\bar{\omega}_s^{\,2}+k_{XX}+j\bar{\omega}_s c_{XX} & k_{XY}+j\bar{\omega}_s c_{XY}\\ k_{YX}+j\bar{\omega}_s c_{YX} & -\bar{M}_s\bar{\omega}_s^{\,2}+k_{YY}+j\bar{\omega}_s c_{YY}\end{bmatrix}\begin{bmatrix}X\\ Y\end{bmatrix}=\begin{bmatrix}0\\ 0\end{bmatrix} \quad (6)$$

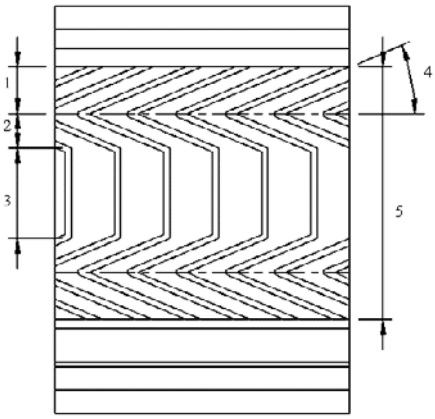
The neutral stability criterion for the solution of Eq. (6) requires the determination of the system to be zero. Equations (7) and (8) express the real part and imaginary parts, respectively:

$$\bar{\omega}_s^2=\frac{(k_{eq}-k_{XX})(k_{eq}-k_{YY})-k_{XY}k_{YX}}{c_{XX}c_{YY}-c_{XY}c_{YX}}=\left(\frac{\omega_s}{\Omega_s}\right)^2 \quad (7)$$

https://doi.org/10.1017/jmech.2012.13 Published online by Cambridge University Press

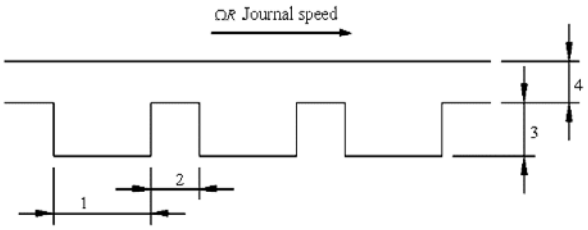


(a) Herringbone-microgrooved journal bearing pattern



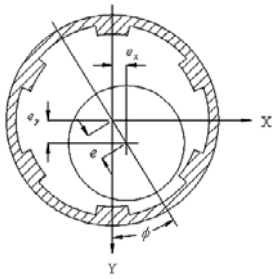
1. L_1: upper groove length 2. L_2: lower groove length 3. L_3: free groove length 4. β: groove angle 5. L: width of journal bearing

(b) Unwrapped geometry



1. W_g: groove width 2. W_r: ridge width 3. C_g: groove depth 4. C: radial clearance of journal bearing

(c) Ridge-groove pair



(d) The considered coordinate system

Fig. 3 Geometry parameters of the herringbone-microgrooved journal bearing

$$\bar{M}_s\,\bar{\omega}_s^{\,2} = k_{eq} = \frac{k_{XX}c_{YY} + k_{YY}c_{XX} - c_{YX}k_{XY} - c_{XY}k_{YX}}{c_{XX} + c_{YY}} = \frac{CM\omega_s^{\,2}}{W} \tag{8}$$

For a given Sommerfeld number, calculating the dimensionless equivalent stiffness k_{eq} can retrieve the threshold of whirl frequency ratio $\bar{\omega}_s$. This substitution yields the dimensionless critical mass:

$$\bar{M}_s = k_{eq} / \bar{\omega}_s^2 \tag{9}$$

which agrees with the threshold speed of rotation Ω_s. The dimensionless threshold speed of rotation can be defined as:

$$\bar{\Omega}_s = \sqrt{\bar{M}_s} = \Omega_s \sqrt{\frac{MC}{W}} \tag{10}$$

Evaluating the dimensionless critical mass that is a function of dynamic coefficients can enable stability analysis. The dimensionless threshold speed of rotation represents the threshold stability of the impeller-spindle. Equation (8) shows that equivalent stiffness k_{eq} is:

$$K_{eq} = k_{eq}\left(\frac{W}{C}\right) = M\omega_s^2 \tag{11}$$

Therefore, the natural frequency of the impeller- spindle supported on a herringbone-microgrooved journal bearing is represented as

$$\omega_n = \sqrt{\frac{K_{eq}}{M}} = \omega_s \tag{12}$$

The operation conditions of the Sommerfeld number were defined first. The conditions include the rated operating conditions (speed, lubricant viscosity, static load, and geometry parameters), and provide a relation to determine the particular equilibrium at the operating journal eccentricity ratio, required to generate the film reaction balancing the externally applied static load. Therefore, the static characteristics are related to the unique dimensionless Sommerfeld number. By experimental methodology [17-19] and the following procedures, the dimensionless force coefficients, stiffness k_{ij} and damping c_{ij}, are functions of the Sommerfeld number for stability analysis.

3.2 Determination of Stiffness Coefficients Using the Incremental Static Load Method

The increments in static force applied to lubricant film, ΔF_X and ΔF_Y in the X and Y directions, are related to the changes in shaft displacement relative to its equilibrium location in X and Y directions by four coefficients of stiffness. Equation (13) presents the relation in matrix form:

$$\begin{bmatrix}\Delta F_X \\ \Delta F_Y\end{bmatrix} = \begin{bmatrix}K_{XX} & K_{XY} \\ K_{YX} & K_{YY}\end{bmatrix}\begin{bmatrix}\Delta x \\ \Delta y\end{bmatrix} \tag{13}$$

If the [K] matrix is inverted, Eq. (13) can be written as:

$$[\Delta D] = [K]^{-1}[\Delta F] \tag{14}$$

or more explicitly as:

https://doi.org/10.1017/jmech.2012.13 Published online by Cambridge University Press

$$\begin{bmatrix}\Delta x\\ \Delta y\end{bmatrix}=\begin{bmatrix}K_{XX} & K_{XY}\\ K_{YX} & K_{YY}\end{bmatrix}^{-1}\begin{bmatrix}\Delta F_X\\ \Delta F_Y\end{bmatrix}=\begin{bmatrix}a_{XX} & a_{XY}\\ a_{YX} & a_{YY}\end{bmatrix}\begin{bmatrix}\Delta F_X\\ \Delta F_Y\end{bmatrix} \quad (15)$$

where the quantities a_{XX}, a_{XY}, a_{YX}, a_{YY} are the oil-film influence coefficients. This approach simply applies a load in one direction only, and measures the resulting displacements in directions. The constructed test rig is capable of providing loads on the bearing in X and Y directions, as shown in Fig. 4. If the force in the Y direction is zero, the influence coefficient approach obtains the following simple relationships:

$$a_{XX}=\frac{\Delta x}{\Delta F_X};\quad a_{YX}=\frac{\Delta y}{\Delta F_X} \quad (16)$$

Similarly, when the force in the X direction is zero,

$$a_{XY}=\frac{\Delta x}{\Delta F_Y};\quad a_{YY}=\frac{\Delta y}{\Delta F_Y} \quad (17)$$

Using this approach to determine all of the elements in the influence coefficients, matrix $[K]^{-1}$ is re-inverted to determine the values of the oil-film stiffness coefficients.

3.3 Determination of Damping Coefficients by Using the Unbalance-Excitation Method

The unbalanced-excitation method enables determining the bearing's oil-film damping coefficients after retrieving the bearing stiffness coefficients described in Section 3.2. The rotor mass M is subject to a known imbalance force of magnitude f, provided by attaching an imbalance mass m to the rotor 20mm distant from the rotor center. This mass imbalance is large enough to ensure that any other residual imbalance in the impeller-spindle is insignificantly small in comparison. Because this imbalance provides excitation, the corresponding forces on the rotor in the X and Y directions are one quarter of a revolution out of phase with each other. These forces can be written as follows:

$$f_X=f\sin\Omega t;\quad f_Y=f\cos\Omega t;\quad f=mr_i\Omega^2 \quad (18)$$

In addition to the imbalance forces, the rotor has oil-film forces acting on it. The journal transmits these forces to the rotor, acting in opposite motion of the journal, away from its steady position. The equations of motion in the X direction, and Y direction can be written as:

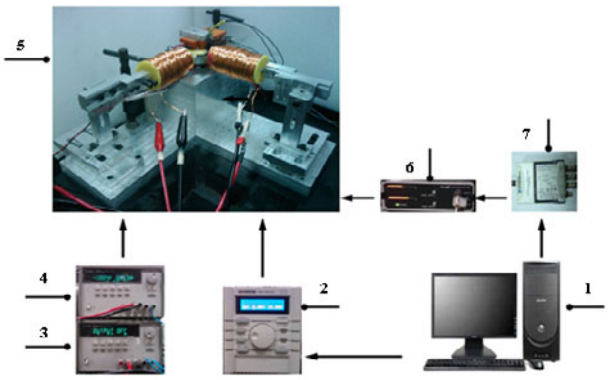
$$f\sin\Omega t-K_{XX}x-K_{XY}y-C_{XX}\dot{x}-C_{XY}\dot{y}=M\ddot{x} \quad (19)$$

$$f\cos\Omega t-K_{YX}x-K_{YY}y-C_{YX}\dot{x}-C_{YY}\dot{y}=M\ddot{y} \quad (20)$$

The displacements of the journal relative to the bearing take the form:

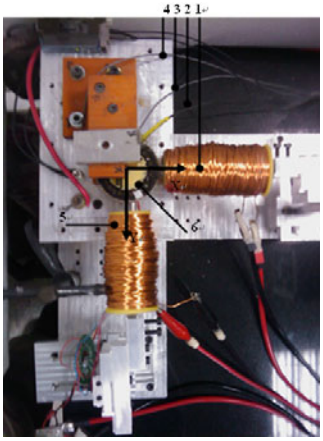
$$x=X\sin(\Omega t-\alpha_1);\quad y=Y\cos(\Omega t-\alpha_2) \quad (21)$$

Equation (21) can be differentiated with respect to time, to obtain expressions for $\dot{x},\dot{y},\ddot{x},\ddot{y}$ and substitute into Eqs. (19) and (20). Solving the damping coefficients requires transforming the matrix, as follows:



1. PC 2. Power supply for impeller-spindle 3. Power supply to apply an Electromagnetic force in the X direction 4. Power supply to apply an Electromagnetic force in the Y direction 5. Measurement platform 6. Capacitance displacement meter 7. NI DAQ-NI 9215 card

(a) Experiment apparatus



1. Electromagnetic force in the X direction 2. Optical fiber trigger 3. Capacitance probe for the Y direction 4. Capacitance probe for the X direction 5. Electromagnetic force in the Y direction 6. Impeller-spindle

(b) Measurement platform

Fig. 4 Schematic of experimental setup

$$\begin{bmatrix}X\Omega\sin\alpha_1 & -Y\Omega\cos\alpha_2 & 0 & 0\\ X\Omega\cos\alpha_1 & Y\Omega\sin\alpha_2 & 0 & 0\\ 0 & 0 & X\Omega\cos\alpha_1 & Y\Omega\sin\alpha_2\\ 0 & 0 & X\Omega\sin\alpha_1 & -Y\Omega\cos\alpha_2\end{bmatrix}\begin{bmatrix}C_{XX}\\ C_{XY}\\ C_{YX}\\ C_{YY}\end{bmatrix}$$
$$=\begin{bmatrix}f+M\Omega^2X\cos\alpha_1-K_{XX}X\cos\alpha_1-K_{XY}Y\sin\alpha_2\\ -M\Omega^2X\sin\alpha_1+K_{XX}X\sin\alpha_1-K_{XY}Y\cos\alpha_2\\ f+M\Omega^2Y\sin\alpha_2+K_{YX}X\sin\alpha_1-K_{YY}Y\cos\alpha_2\\ M\Omega^2Y\sin\alpha_2-K_{YX}X\cos\alpha_1-K_{YY}Y\sin\alpha_2\end{bmatrix} \quad (22)$$

Experimental measurements determine the concerned quantities in Eq. (22). Thus, this approach obtains the damping coefficients.

4. EXPERIMENTAL APPARATUS AND PROCEDURES UNDER RATED OPERATING CONDITIONS

Figure 4 shows the device designed and constructed for experimental investigation. To simulate the static

https://doi.org/10.1017/jmech.2012.13 Published online by Cambridge University Press

loads, the investigation involved applying electromagnetic forces to the metal ring on the impeller-spindle at a specific speed, to generate attractive forces in the radial direction. A capacitance sensor with a 0.025μm/mV sensitivity was applied to measure the static displacement of journal eccentricity relative to the bearing in the *X* and *Y* directions. Data was recorded using an *A*/*D* converter with 16-bit resolution based on a NI DAQ-NI 9215 card with BNC connectors for Hi-Speed USB data transfer. This converter was also constructed with a set of master programs developed in "LabVIEW" platform. And applied "MATLAB" software to calculate bearing dynamic coefficients for stability analysis.

The P-Q curve of impeller-spindle applied to NB, AIO, and tablet PC is similar to Fig. 5. The intersection of the P-Q performance curve and system impedance curve indicate the operating point of the impeller- spindle. For given rated operating conditions, the Sommerfeld numbers are determined first, since the bearing geometry parameters, speeds, viscosity, and loads are already known. The measured temperature of the internal fluid film increased about 4°C, which is less than 7% variation due to the operation, from a range of 2700 to 4900rpm. This small variation maintains the lubricant viscosity approximately constant. Figure 6 illustrates the various static loads relative to different operating speeds of the impeller-spindle, with respect to twelve Sommerfeld numbers. Regarding the methodology in sections 3.2 and 3.3, this study's experiment measured static and dynamic coefficients for impeller-spindle with a herringbone-microgrooved journal bearing over all the defined Sommerfeld numbers under the rated operating conditions listed below. The rotor maintained constant speeds at 2700, 3600, 4200, and 4900rpm, and each impeller-spindle speed varied with electromagnetic forces of 0.4, 0.8, and 1.6N, relative to various static loads. Once the impeller- spindle reached the required steady state at each speed with one concerned static load, the master programs in the "LabVIEW" platform recorded the following data:

(1) incremental displacement of journal, relative to the equilibrium position in *X* and *Y* direction, Δx; Δy

(2) rotational speed of journal, Ω

(3) static load applied by electromagnetic force, *W*

(4) displacement of journal, relative to the equilibrium position in *X* and *Y* direction, *x*; *y*

Following the data acquisition in steps (1), (2), and (3) with the method of incremental static load described in Section 3.2 and the data acquisition of step (4) with unbalanced excitation method in Section 3.3, the dynamic coefficients can be obtained by applying the "MATLAB" software. Repeating these data acquisition procedures with an increased static load while maintaining constant rotor speed enables to calculate the other dynamic coefficients until three kinds of static loads were measured. All tests were repeated with other rotor speeds and aforementioned procedures systematically until the four rotor speeds were reached.

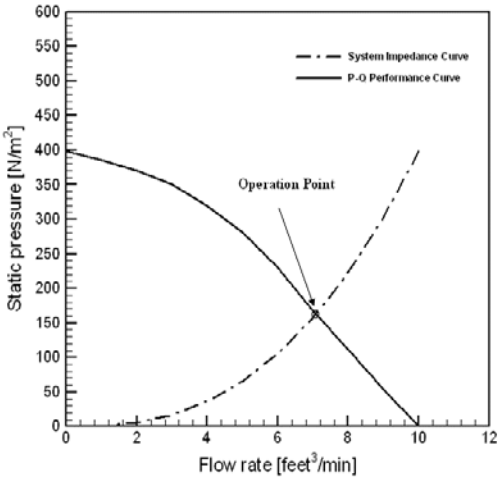


Fig. 5 Operation point of impeller-spindle

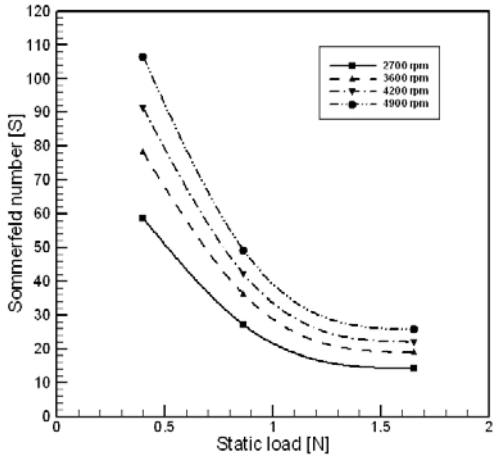


Fig. 6 Sommerfeld numbers related to specific static load and four rotational speeds

5. RESULTS AND DISCUSSION

This study evaluates various operating points corresponding to twelve values of the Sommerfeld numbers for stability analysis. The error bars in the related figures represent the uncertainty in the results calculated for uncertainty analysis [20,21]. Uncertainty analysis shows that the maximum uncertainty of the eccentricity ratio is ±5.2% of its mean value. The maximum uncertainty of dimensionless stiffness coefficients and dimensionless damping coefficients are ±5.2% and ±5.6% of their mean value, respectively.

5.1 Analysis of Static Characteristics

Figure 7 presents the variation of the eccentricity ratio with static loads of 0.4, 0.8, and 1.6N. A higher rotating speed of the journal leads to a lower eccentricity ratio under the same static load because the film force is proportional to journal speed. As rotation speed increases, the journal gradually approaches the bearing center because it requires less of a convergent wedge effect to support the same static load. Figure 8

https://doi.org/10.1017/jmech.2012.13 Published online by Cambridge University Press

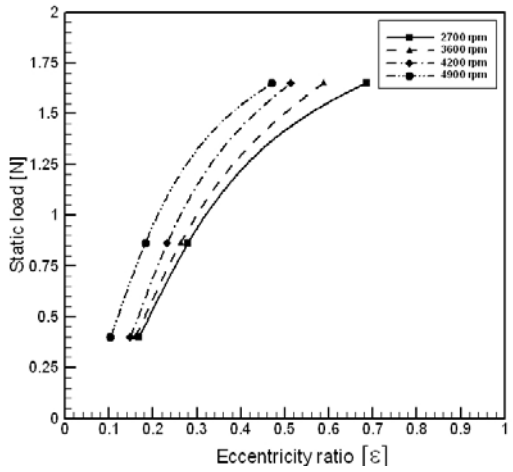


Fig. 7 Variation of the static loads corresponding to different rotating speeds with eccentricity ratio

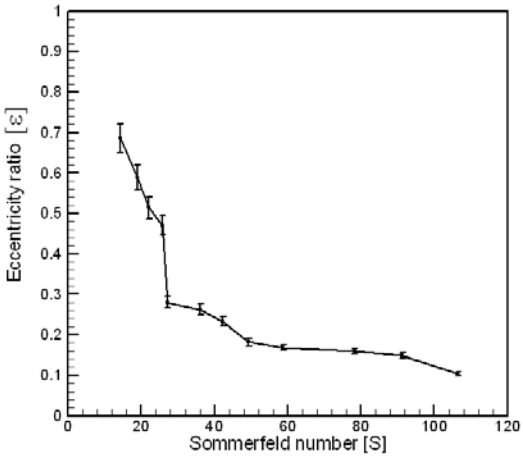


Fig. 8 Variation of the eccentricity ratio with the Sommerfeld number

provides a relation to determine the equilibrium eccentricity ratio with respect to Sommerfeld numbers, indicating that the eccentricity ratio become smaller as the Sommerfeld number increases.

5.2 Analysis of Dynamic Coefficients for Dimensionless Stiffness and Damping Coefficients

Figure 9 shows the variation of dimensionless stiffness coefficients with Sommerfeld numbers, indicating that the dimensionless direct stiffness coefficients of k_{XX} and k_{YY} are positively correlated to the Sommerfeld number. The groove effect might be responsible, which gradually replaces the wedge effect as the dominant effect with the decreasing of the eccentricity ratio, and reaches a maximum value at nearly the concentric position of the bearing. This behavior is unlike that of a plain journal bearing, and follows trends presented by Rao *et al*. [8]. As a result, the dimensionless direct stiffness provides an increasing restoring force that pushes the journal back toward its steady-state equilibrium position as the Sommerfeld number increases. The magnitude of this stiffness governs the location and

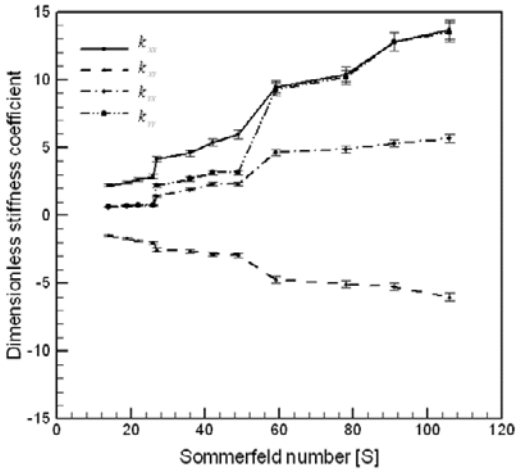


Fig. 9 Variation of the dimensionless stiffness coefficient with increasing Sommerfeld number

amplification of the rotor's critical speed. The dimensionless direct stiffness coefficients also become close as the Sommerfeld number increases from 59 to 106. This symmetry of dimensionless direct stiffness coefficients are usually preferred to unbalance response considerations because the journal attains a circular orbital shape, not beneficial for stability. The skew-symmetry of the dimensionless cross-coupled stiffness k_{XY} and k_{YX} increases alongside the Sommerfeld number, and combines a force that is gradually collinear with the whirl direction, to promote journal vibration. The dimensionless cross-coupled stiffness gradually becomes smaller as the Sommerfeld number decreases. This illustrates that the combination of the forward tangential force gradually decreases with the increase of the eccentricity ratio. Dimensionless direct damping coefficients are often the predominant source of damping, and primarily dictate the unbalance response and rotor stability. Figure 10 indicates that the dimensionless direct damping coefficients of c_{XX} and c_{YY} become larger as the Sommerfeld number increases. The combination of these two direct damping coefficients c_{XX} and c_{YY} produces a force that is tangential to the vibration orbit against the whirling motion.

5.3 Stability Analysis

5.3.1 Characteristics of Threshold of Whirl Frequency Ratio $\bar{\omega}_s$

Figure 11 illustrates the threshold of whirl frequency ratio characteristics at a given Sommerfeld number. The threshold of whirl frequency ratio increases alongside the Sommerfeld number, and this increase displays asymptotic flatness when the Sommerfeld number exceeds a value of 59. The flatness section indicates that the threshold of whirl frequency ratio approaches a value of 0.81 to 0.88. The threshold of whirl frequency ratio approaches a value of 0.6 when the Sommerfeld number is 49, and the maximum rotational speed of the journal can attain nearly $1.67\omega_s$. The squared values of the threshold of whirl frequency ratio are positive for all Sommerfeld numbers, signifying that the impeller-spindle can result in instability under

https://doi.org/10.1017/jmech.2012.13 Published online by Cambridge University Press

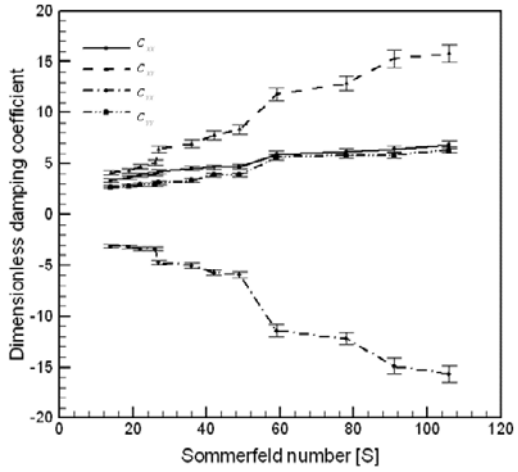


Fig. 10 Variation of the dimensionless damping coefficient with increasing Sommerfeld number

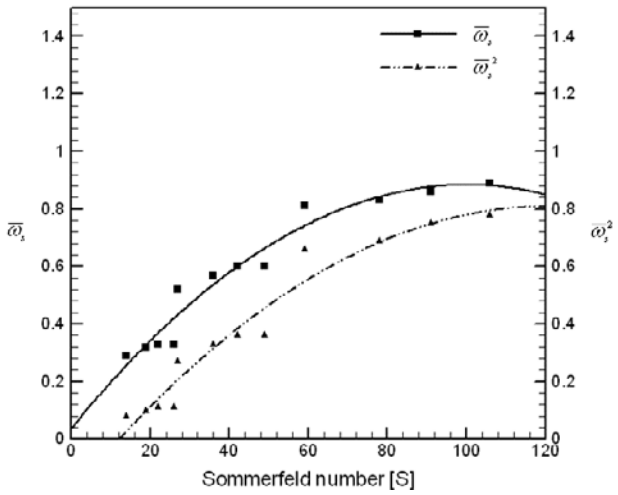


Fig. 11 Variation of the threshold of whirl frequency ratio $\bar{\omega}_s$ and the squared values of the threshold of whirl frequency ratio $\bar{\omega}_s^2$ with respect to the Sommerfeld number

certain operating conditions. In contrast, if the threshold of whirl frequency ratio can take an imaginary value, the characteristic equation of the system would not have any root at the imaginary axis. Thus, a negative squared value of the threshold of whirl frequency ratio indicates that the operation is stable for any rotating speed at any mass.

5.3.2 Threshold speed of rotation Ω_s and dimensionless threshold speed of rotation $\bar{\Omega}_s$

Figure 12 shows the threshold speed of the rotation Ω_s, which is the lowest rotating speed, and the dimensionless threshold speed of the rotation $\bar{\Omega}_s$, with respect to the Sommerfeld numbers. The impeller-spindle operating at a lower static load with a higher rotating speed, that is, a large Sommerfeld number, has a lower criterion of threshold speed of the rotation Ω_s. When the Sommerfeld number is 49, the threshold

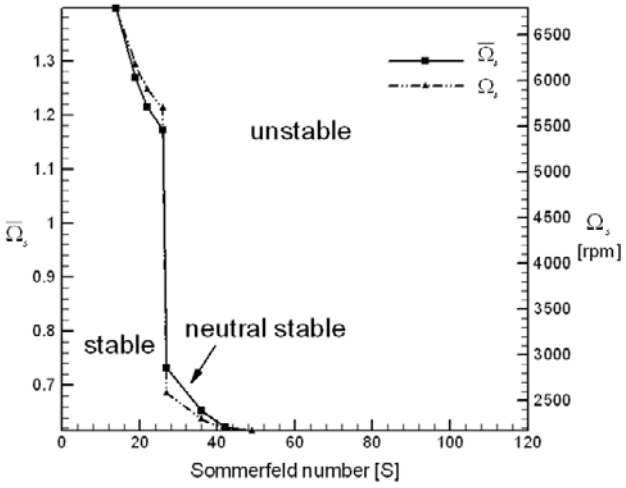


Fig. 12 Variation of the threshold speed of the rotation Ω_s and the dimensionless threshold speed of the rotation $\bar{\Omega}_s$ with respect to the Sommerfeld number

speed of the rotation Ω_s is 2162rad/s. After calculating the value of $\bar{\Omega}_s$, it is possible to obtain the stability boundary of the dimensionless threshold speed of rotation $\bar{\Omega}_s$. This boundary indicates that the impeller-spindle is neutrally stable in operation, as shown in Fig. 12. Below the value of stability boundary and Sommerfeld numbers from 14 to 49, all four eigenvalues have negative real parts, and the impeller-spindle is stable. Above the value of stability boundary and Sommerfeld numbers from 49 to 106, the impeller-spindle becomes unstable.

5.3.3 Dimensionless equivalent stiffness k_{eq}, dimensionless critical mass $\bar{M}_s$, and dimensionless mass $\bar{M}$

The dimensionless equivalent stiffness k_{eq} values in Fig. 13 display a change from positive to negative when the Sommerfeld number is from the value of 49 to 59 at a rated operating condition. The squared values of the threshold of whirl frequency ratio are positive with all Sommerfeld numbers in Section 5.3.1, signifying that the dimensionless critical mass $\bar{M}_s$ in Fig. 13 becomes negative when the Sommerfeld number exceeds the value of 49. The rotational speed intervenes in the definition of the dimensionless critical mass, as in Eq. (9); therefore, determining a critical mass is equivalent to determining the rotation speed for a given geometry of a herringbone-microgrooved journal bearing. Figure 14 shows the stability using a curve representing the variation, with respect to the ratio of the dimensionless critical mass $\bar{M}_s$ to the dimensionless mass $\bar{M}$. The impeller-spindle is stable when the ratio of $\bar{M}_s / \bar{M}$ is greater than 1 when Sommerfeld number is less than 59. On the other hand, the impeller-spindle becomes unstable when the ratio of $\bar{M}_s / \bar{M}$ is less than 1 for Sommerfeld number from 59 to 106. It shows that the impeller-spindle should not operate

https://doi.org/10.1017/jmech.2012.13 Published online by Cambridge University Press

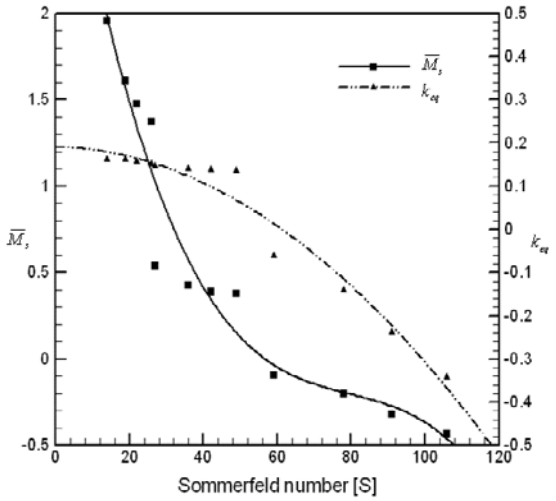


Fig. 13 Variation of the dimensionless critical mass $\bar{M}_s$ and the dimensionless equivalent stiffness k_{eq} with the Sommerfeld number

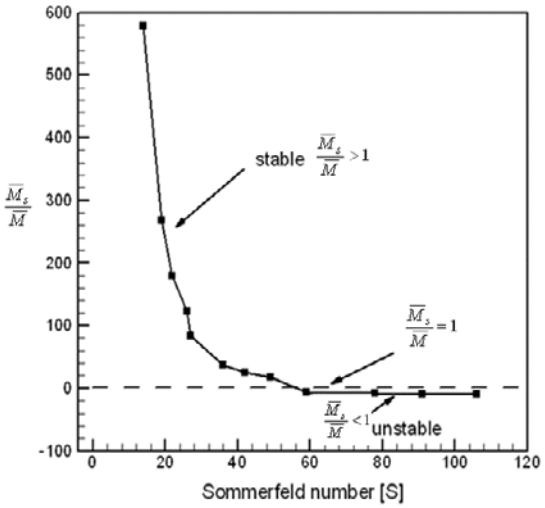


Fig. 14 Variation of ratio of the dimensionless critical mass $\bar{M}_s$ to the dimensionless mass $\bar{M}$ with the Sommerfeld number

below the equilibrium eccentricity ratio at values of 0.18 as Fig. 8. For a negative value of $\bar{M}_s$ and a positive coefficient of $\bar{\omega}_s^2$, the impeller-spindle becomes unstable for any value of the dimensionless mass $\bar{M}$.

The dimensionless critical mass $\bar{M}_s$ is dependent on the dynamic coefficients. The stability could be attributed, as shown in Figs. 9 and 10 because the effective force following dimensionless direct damping coefficients is larger than the contribution by the dimensionless cross-coupled stiffness with Sommerfeld numbers from 14 to 49. For Sommerfeld numbers from 59 to 106, the dimensionless cross-coupled stiffness combines to create a force pointing in the whirl direction, destabilizing the impeller-spindle because the dimensionless direct damping force is unable to dissipate the energy injected by the cross-coupled stiffness force.

5.3.4 Natural Frequency ω_n, Threshold of Whirl Frequency ω_s, and Rotation Speed of Journal Ω

Figure 15 shows that the natural frequency's variation of the impeller-spindle decreases with the increase of the Sommerfeld number. The maximum rotational speed the journal can attain is nearly $1.67\omega_n$ as shown in Section 5.3.1. For a rated operating condition of the Sommerfeld number being greater than 49 and the eccentricity ratio being less than 0.18, the natural frequency of the impeller-spindle is an imaginary value due to the negative k_{eq} and the impeller-spindle whirling at all speeds.

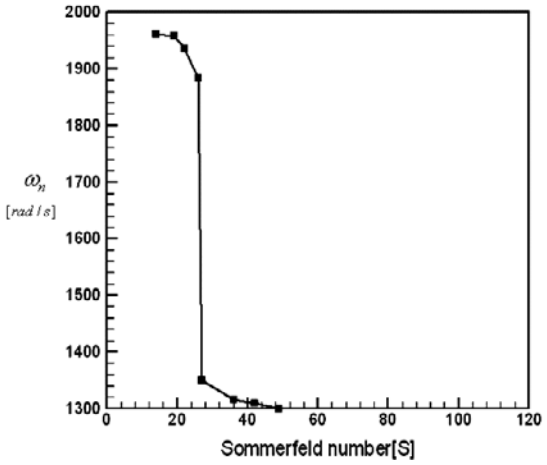


Fig. 15 Variation of the natural frequency ω_n of the impeller-spindle versus the Sommerfeld number

6. CONCLUSIONS

This study experimentally investigates the stability of an impeller-spindle supported by a herringbone-microgrooved journal bearing . Experiments at 2700, 3600, 4200, and 4900rpm with static loads ranging from 0.4 to 1.6 N reveal the following conclusions:

1. The threshold of whirl frequency ratio increases alongside the Sommerfeld number. The threshold of whirl frequency ratio approaches a value of 0.6 when the Sommerfeld number is 49, and the maximum rotational speed the journal can attain is nearly $1.67\omega_s$ and $1.67\omega_n$.
2. The threshold speed of the rotation Ω_s and the dimensionless threshold speed of the rotation $\bar{\Omega}_s$ are negatively correlated with the Sommerfeld number. When the Sommerfeld number is 49, the threshold speed of the rotation Ω_s is 2162rad/s. Below the value $\bar{\Omega}_s$ of the stability boundary and Sommerfeld numbers from 14 to 49, the impeller- spindle is stable. Above the value $\bar{\Omega}_s$ of the stability boundary and Sommerfeld numbers from 49 to 106, the impeller-spindle becomes unstable.
3. The impeller-spindle is stable when the ratio of

https://doi.org/10.1017/jmech.2012.13 Published online by Cambridge University Press

$\bar{M}_s / \bar{M}$ is greater than 1, with the Sommerfeld number ranging from 49 to 14. The motor becomes unstable when the ratio of $\bar{M}_s / \bar{M}$ is less than 1, with the Sommerfeld number ranging from 59 to 106. Thus, the impeller-spindle should not operate below the equilibrium eccentricity ratio at values of 0.18.

4. The impeller-spindle whirls at all speeds for a rated operating condition with the Sommerfeld number ranging from 59 to 106.

In summation, it is necessary to determine whether an impeller-spindle with a herringbone-microgrooved journal bearing, operating at a lightly static load with a higher rotating speed is within the stability region. The passive control method with a designed magnet force in a bearing's inner diameter circumference as a preload for increasing impeller-spindle's eccentricity might prove useful to achieve stability.

NOMENCLATURES

a_{XX}, a_{XY}, a_{YX}, a_{YY} oil-film influence coefficients [m/N]

C radial clearance of journal bearing [μm]

C_g groove depth [μm]

C_{ij}, C_{XX}, C_{XY}, C_{YX}, C_{YY} damping coefficients [N·s/m]

c_{ij}, c_{XX}, c_{XY}, c_{YX}, c_{YY} dimensionless damping coefficients

D diameter of journal [mm]

e_x eccentricity in X direction [μm]

e_y eccentricity in Y direction [μm]

e eccentricity [μm]

f imbalance force [N]

f_X imbalance force in X direction [N]

f_Y imbalance force in Y direction [N]

K_{eq} equivalent stiffness of impeller-spindle [N/m]

K_{ij}, K_{XX}, K_{XY}, K_{YX}, K_{YY} stiffness coefficients [N/m]

$[K]$ stiffness coefficients matrix

$[K]^{-1}$ invert matrix of stiffness coefficients matrix

k_{eq} dimensionless equivalent stiffness of impeller-spindle

k_{ij}, k_{XX}, k_{XY}, k_{YX}, k_{YY} dimensionless stiffness coefficients

L width of journal bearing [mm]

L_1 upper groove length [mm]

L_2 lower groove length [mm]

L_3 free groove length [mm]

M rotor mass [g]

$\bar{M}$ dimensionless mass

$\bar{M}_s$ dimensionless critical mass

m residual imbalance mass of impeller-spindle [mg]

N_g number of groove

R radius of journal [mm]

r_c eccentricity of gravity center of impeller-spindle [mm]

r_i radius of imbalance mass [mm]

S Sommerfeld number ($= \frac{\mu NLD}{W}\left(\frac{R}{C}\right)^2$)

U surface velocity of the journal [m/s]

W static load [N]

W_g groove width [μm]

W_r ridge width [μm]

X inertial coordinate system in the X direction

X amplitude of orbit motion in the X direction [μm]

x displacement of journal relative to the bearing in X direction [μm]

$\dot{x}$, $\ddot{x}$ velocity and acceleration of journal relative to the bearing in X direction [μm/s, μm/s^2]

$\bar{x}$ dimensionless variable in displacement of X direction

Y inertial coordinate system in the Y direction

Y amplitude of orbit motion in the Y direction [μm]

y displacement of journal relative to the bearing in Y direction [μm]

$\dot{y}$, $\ddot{y}$ velocity and acceleration of journal relative to the bearing in Y direction [μm/s, μm/s^2]

$\bar{y}$ dimensionless variable in displacement of Y direction

Greek Symbols

α_1 phase angle of X directional displacement [°]

α_2 phase angle of Y directional displacement [°]

β groove angle [°]

$[\Delta D]$ relative displacement matrix

ΔF_X increment of static load in X direction [N]

ΔF_Y increment of static load in Y direction [N]

https://doi.org/10.1017/jmech.2012.13 Published online by Cambridge University Press

$[\Delta F]$ increasing static load matrix

Δx increment of displacement of journal relative to the bearing in X direction [μm]

Δy increment of displacement of journal relative to the bearing in Y direction [μm]

ε eccentricity ratio

μ dynamic viscosity of the lubricant [kg/m-s]

τ dimensionless time

ϕ attitude angle $[^\circ]$

Ω rotational speed of journal [rad/s]

Ω_s threshold speed of rotation [rad/s]

$\bar{\Omega}_s$ dimensionless threshold speed of rotation

ω_s threshold of whirl frequency [rad/s]

ω_n natural frequency of impeller-spindle [rad/s]

$\bar{\omega}_s$ threshold of whirl frequency ratio

REFERENCES

1. Matsuda, K., Kijimoto, S. and Kanemitsu, Y., "Stability-Optimized Clearance Configuration of Fluid-Film Bearings," *Journal of Tribology*, ASME, **129**, pp. 106–111 (2007).
2. Ono, K., Murashita, S. and Yamaura, H., "Stability Analysis of a Disk-Spindle Supported by a Plain Journal Bearing and Pivot Bearing," *Microsystem Technologies*, **11**, pp. 734–740 (2005).
3. Zhou, H., Zhao, S., Xu, H. and Zhu, J., "An Experimental Study on Oil-Film Dynamic Coefficients," *Tribology International*, **37**, pp. 245–253 (2004).
4. Ertas, B. and Vance, J., "The Influence of Same-Sign Cross-Coupled Stiffness on Rotordynamics," *Journal of Vibration Acoustics*, ASME, **129**, pp. 24–31 (2007).
5. Jang, G. H. and Yoon, J. W., "Nonlinear Dynamic Analysis of a Hydrodynamic Journal Bearing Considering the Effect of a Rotating or Stationary Herringbone Groove," *Journal of Tribology*, ASME, **124**, pp. 277–304 (2002).
6. Jang, G. H. and Yoon J. W., "Stability Analysis of a Hydrodynamic Journal Bearing with Rotating Herringbone Grooves," *Journal of Tribology*, ASME, **125**, pp. 291–300 (2003).
7. Hwang, T. and Ono, K., "Analysis and Design of Hydrodynamic Journal Air Bearings for High Performance HDD Spindle," *Microsystem Technologies*, **9**, pp. 386–394 (2003).
8. Rao, T. V. V. L. N. and Sawicki, J. T., "Stability Characteristics of Herringbone Grooved Journal Bearings Incorporating Cavitation Effects," *Journal of Tribology*, ASME, **126**, pp. 281–287 (2004).
9. Chu, L. M., Li, W. L., Shen, R. W. and Tsia, T. I., "Dynamic Characteristics of Grooved Air Bearings in Microsystem," *Proceedings of the Institution of Mechanical Engineers, Part J: Journal of Engineering Tribology*, **223**, pp. 895–908 (2009).
10. Jintanawan, T., "Vibration of Hard Disk Drive Spindle Systems with Distributed Journal Bearing Forces," *Microsystem Technologies*, **12**, pp. 208–218 (2006).
11. Miwa, M., Miyazaki, H., Kaneko, R. and Unozawa, H., "Evaluation of Fluid Dynamic Bearing Spindle by Vibration Base," *IEEE Transactions on Magnetics*, **41**, pp. 763–768 (2005).
12. Jang, G. H. and Lee, C. I., "Development of an HDD Spindle Motor with Increased Stiffness and Damping Coefficients by Utilizing a Stationary Permanent Magnet," *IEEE Transactions on Magnetics*, **43**, pp. 2570–2572 (2007).
13. Nemat-Alla, M. M., Gad, A. M., Khalil, A. A. and Nasr, A. M., "Static and Dynamic Characteristics of Oil Lubricated Beveled-Step Herringbone-Grooved Journal Bearings," *Journal of Tribology*, ASME, **131**, pp. 011701-1–011701-7 (2009).
14. Liu, C. S., Tsai, M. C., Yen, R. H., Lin, P. D. and Chen, C. Y., "Design and Experimental Verification of Novel Hydrodynamic Grooved Journal Bearing," *Journal of the Chinese Society of Mechanical Engineers*, **31-2**, pp. 139–146 (2010).
15. Hamrock, B. J., Schmid, S. R. and Jacobson, B. O., *Fundamentals of Fluid Film Lubrication*, 2nd Edition, Marcel Dekker, New York, U.S.A., pp. 287–393 (2004).
16. San Andrés, L., "Hydrodynamic Fluid Film Bearings and Their Effect on the Stability of Rotating Machinery," *Design and Analysis of High Speed Pumps*, pp. 10-1–10-36 (2006).
17. Goodwin, M. J., *Dynamics of Rotor-Bearing System*, Unwin Hyman Inc. (1989).
18. Nikolakopoulos, P. G. and Papadopoulos, C. A., "Controllable High Speed Journal Bearings Lubricated with Electrorhelolgical Fluids—An Analytical and Experiment Approach," *Tribology International*, **31**, pp. 225–234 (1998).
19. Tiwari, R., Lees, A. W. and Friswell, M. I., "Identification of Dynamic Bearing Parameters: A Review," *The Shock and Vibration Digest*, **36**, pp. 99–124 (2004).
20. Bell, S., *A Beginner's Guide to Uncertainty of Measurement*, ISSN 1368-6550 (2001).
21. *Guide to the Expression of Uncertainty in Measurement*, ISO, Geneva, Switzerland (1995).

(Manuscript received November 17, 2010, accepted for publication April 28, 2011.)

https://doi.org/10.1017/jmech.2012.13 Published online by Cambridge University Press